Dentomaxillofacial Radiology (2007) 36, 328–335
© 2007 The British Institute of Radiology
http://dmfr.birjournals.org

RESEARCH

Content-based access to oral and maxillofacial radiographs

TM Deserno*[,1], B Molander[2], MO Güld[1], C Thies[1] and H-G Gröndahl[2]

[1]Department of Medical Informatics, Aachen University of Technology (RWTH), Aachen, Germany; [2]Department of Oral and Maxillofacial Radiology, The Sahlgrenska Academy, Göteborg University, Göteborg, Sweden

Objectives: Content-based access (CBA) to medical image archives, *i.e.* data retrieval by means of image-based numerical features computed automatically, has capabilities to improve diagnostics, research and education. In this study, the applicability of CBA methods in dentomaxillofacial radiology is evaluated.

Methods: Recent research has discovered numerical features that were successfully applied for an automatic categorization of radiographs. In our experiments, oral and maxillofacial radiographs were obtained from the day-to-day routine of a university hospital and labelled by an experienced dental radiologist regarding the technique and direction of imaging, as well as the displayed anatomy and biosystem. In total, 2000 radiographs of 71 classes with at least 10 samples per class were analysed. A combination of co-occurrence-based texture features and correlation-based similarity measures was used in leaving-one-out experiments for automatic classification. The impact of automatic detection and separation of multi-field images and automatic separability of biosystems were analysed.

Results: Automatic categorization yielded error rates of 23.20%, 7.95% and 4.40% with respect to a correct match within the first, fifth and tenth best returns. These figures improved to 23.05%, 7.00%, 4.20%, and 20.05%, 5.65% and 3.25% if automatic decomposition was applied and the classifier was optimized to the dentomaxillofacial imagery, respectively. The dentulous and implant systems were difficult to distinguish. Experiments on non-dental radiographs (10 000 images of 57 classes) yielded 12.6%, 5.6% and 3.6%.

Conclusion: Using the same numerical features as in medical radiology, oral and maxillofacial radiographs can be reliably indexed by global texture features for CBA and data mining.
Dentomaxillofacial Radiology (2007) **36,** 328–335. doi: 10.1259/dmfr/11645252

Keywords: image processing, computer-assisted; medical informatics; radiography, dental, digital; information storage and retrieval

Introduction

In medicine to date, virtually all picture archiving and communication systems (PACS) retrieve images simply by indices based on patient name, imaging modalities, or some alphanumeric description of diagnostic findings. However, for mining or retrieving images for research, diagnostics, or teaching, this methodology of access is certainly limited.[1] Therefore, content-based access (CBA) to medical images, which is also termed content-based image retrieval (CBIR), has become a major topic of research in diagnostic radiology.[2–4]

CBA or CBIR aims at describing the complex object information of digital radiographs by non-textual features that are extracted from the images by means of digital image processing. For instance, colour, texture and shape descriptors are used to represent the entire image or parts within the image.[1,4] In a CBIR system, these numerical features are stored along with the images. According to the query by example (QBE) paradigm,[5] at the time of retrieval, the user presents an example pattern from which the same features are extracted and compared with those hosted in the database. For example, if a radiologist, teacher, or clinician is presented with a panoramic radiograph, such as that in Figure 1a in which a bony lesion of the right side of the mandible is displayed, it is compared with other panoramic radiographs with similar lesions for which the diagnoses are known (Figure 1b,c). This should have obvious advantages both in diagnoses and education.

This comparison relies on appropriate distance measures. Since only a few numbers (usually fewer than

*Correspondence to: Dr Thomas M Deserno, née Lehmann, Institut für Medizinische Informatik der RWTH Aachen, D-52057 Aachen, Germany;
E-mail: deserno@ieee.org
Received 14 June 2006; revised 18 September 2006; accepted 14 October 2006

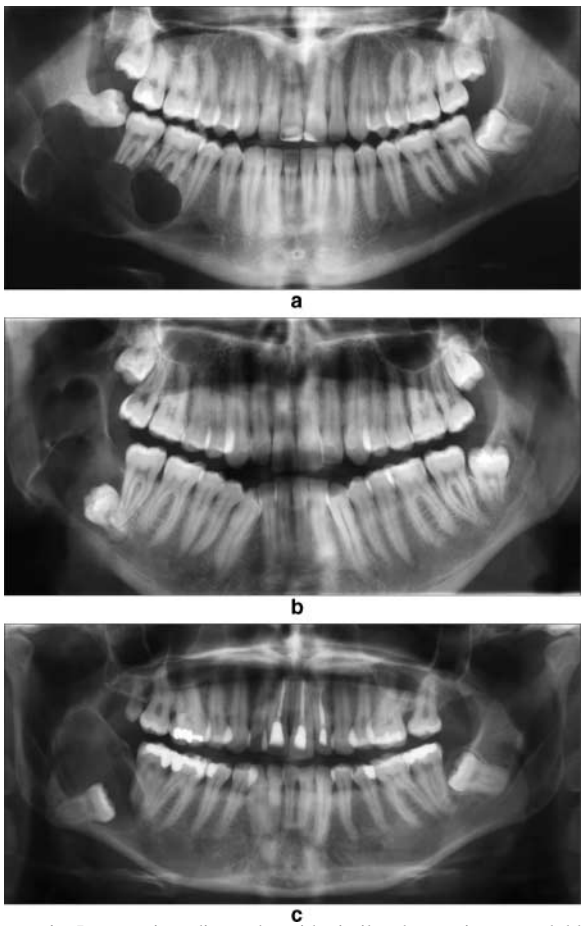

Figure 1 Panoramic radiographs with similar destructions: ameloblastoma (top), keratocyst (middle) and dentigerous cyst (bottom)

1024, which corresponds to 1 KB and 4 KB for an eight-bit integer (char) and float, respectively) are used to represent a digital radiograph (*e.g.* 15 MB for a frontal chest of 3000×4000 pixels and ten-bit grayscales), the comparison of features is much faster than that of the images themselves would be. As response of a CBIR system, the images linked to the most similar feature vectors are presented to the user.

Particular problems with medical CBIR are the absence of colour, which has turned out to be the most discriminative feature in non-medical CBIR applications,[1] and the large diversity of medical patterns. According to the gender, age and body shape of the patient, the settings of the imaging device, positioning of the patient, exposure parameters, pathological alterations and therapeutic instruments, even standardized imaging procedures, deliver highly different image patterns. This is particularly the case for radiographs taken in oral and maxillofacial radiology clinics, described below as dental radiographs. In such radiographs, fillings, implants, or other metallic components are prominent local structures affecting the global appearance of the entire image. Therefore, it is difficult to derive robust numerical features and medical CBIR approaches were excluded from early years of research.[1] In order to reduce this variety, the first CBIR systems applied to medical radiology were specific for certain imaging modalities and special diagnostic contents.[3]

However, recent research has provided numerical features that are suitable for indexing the medical imagery in general.[4,6] In particular, digital image processing is used to extract global image features, *i.e.* a small set of feature numbers (vector) is used to describe the entire image rather than particular image regions. These numerical features are computed automatically from the image pixels. Several techniques are used. Unlike approaches that are based on co-occurrence matrices[7], the Tamura texture measures (TMM[8]) directly capture coarseness, directionality and contrast of an image. Here, a size detector based on the analysis of local averages, properties of image gradients and local variance of pixel intensities are aggregated into one histogram per image and compared using the Jensen–Shannon divergence. Another approach makes use of the cross correlation function (CCF) between the two images, which is calculated from small icons of 8×8 pixels up to 32×32 pixels. The image distortion model (IDM)[9] is a correlation-based feature that also models local deformations.

Another general problem in CBIR research is the evaluation of systems, features, or distance measures with lacking ground truth. Considering global features, such a ground truth has been established by the IRMA group (IRMA, Image Retrieval in Medical Applications, http://irma-project.org).[10,11] According to a multiaxial, mono-hierarchical coding scheme,[9] experienced radiologists uniquely labelled more than 15 000 radiographs that had been arbitrarily collected from clinical routine. In the automatic annotation task of the ImageCLEF 2005 campaign (CLEF, Cross Language Evaluation Forum; http://www.clef-campaign.org), 10 000 radiographs were grouped into 57 classes.[6] Each class contained at least ten images. A subset of 9000 images was released with their class labels for training, while the remaining 1000 radiographs were used for testing. The best error rate was 12.6%. By not considering only the best match, but a number of five or ten response images, which is more appropriate for applications according to the QBE paradigm, the error rates reduced to 5.6% and 3.6%, respectively.

Hence the usability of CBIR techniques for automatic categorization of general radiographs is demonstrated despite the diverse alterations of medical image patterns. It is the basis for local content analysis, which can now be automatically adapted according to the image type as well as the displayed body region.[10] According to Deselaers et al,[12] automatic annotation of medical images is a topic of great importance and relevance to the medical community. Currently, the most relevant areas are:[12]

(1) automatic parameter setting for image analysis[13] to cope with the variety of imaging modalities, appearances of different body regions and the different diagnostic aims;
(2) consistency checks for metadata such as that present in the digital imaging and communications in medicine (DICOM) standard, which is frequently erroneous when generated automatically;[14] and
(3) generation of text queries for information retrieval in picture archiving and communication systems (PACS), which is currently based solely on alphanumerical attributes,[15] *i.e.* text describing the patient, study, etc.

In this study, we investigated whether global texture features can also be applied for automatic annotation of dental radiographs. It is not obvious that the results will be similar to those from medical images: first, dental radiographs may show an even larger diversity of patterns because of fillings, implants and metal crowns, and second, conventional X-ray equipment for extraoral imaging, such as Scanora and Cranex Tome (Soredex, Helsinki, Finland), which is fed with digital sensor plates, produces data files composed of up to eight individual image fields. This partitioning may overlay the relevant patterns within each image field. Also, different categories in terms of meaning might have similar pixel patterns, *e.g.* the dentulous and the implant system, which—in the context of CBIR—is usually referred to as the semantic gap.[1,4]

Materials and methods

A set of 2355 images was selected arbitrarily from the Department of Oral and Maxillofacial Radiology, Göteborg University, Göteborg, Sweden. This image repository reflects the frequency of the imaging procedures applied to the patients. An experienced dental radiologist classified the content of each image using the IRMA coding scheme, which was completed according to the needs in dental practice (Table 1). In particular, (i) the technique of imaging (T-code, four levels of details) and (ii) its direction (D-code, three levels) as well as (iii) the anatomy (A-code, three levels) and (iv) biological system (B-code, three levels) imaged were determined within a monohierarchical standardized terminology.[16]

Table 1 Extended IRMA codes for dental radiology that were used in this study

Code axis	*Position 1*	*Position 2*	*Position 3*	*Position 4*
Technique				
1111	X-ray	Plain radiography	Digital	Overview image
1112	X-ray	Plain radiography	Digital	Tomography
1115	X-ray	Plain radiography	Digital	Far view projection
1119	X-ray	Plain radiography	Digital	Intraoral periapical
111a	X-ray	Plain radiography	Digital	Intraoral bitewing
111b	X-ray	Plain radiography	Digital	Occlusal
111d	X-ray	Plain radiography	Digital	Narrow beam radiography
Direction				
120	Coronal	Anteroposterior (AP, coronal)	Not further specified	
12g	Coronal	Anteroposterior (AP, coronal)	Left side	
12h	Coronal	Anteroposterior (AP, coronal)	Right side	
210	Sagittal	Lateral, right-left	Not further specified	
220	Sagittal	Lateral, left-right	Not further specified	
310	Axial	Craniocaudal	Not further specified	
311	Axial	Craniocaudal	Right adjoining	
312	Axial	Craniocaudal	Left adjoining	
320	Axial	Caudocranial (transversal, axial)	Not further specified	
4c0	Other orientation	Perpendicular to the dental arch	Not further specified	
4c1	Other orientation	Perpendicular to the dental arch	Right adjoining	
4c2	Other orientation	Perpendicular to the dental arch	Left adjoining	
Anatomy				
200	Cranium	Not further specified		
210	Cranium	Facial cranium	Not further specified	
214	Cranium	Facial cranium	Maxilla	
215	Cranium	Facial cranium	Mandible	
216	Cranium	Facial cranium	Temporomandibular area	
217	Cranium	Facial cranium	Paranasal area	
218	Cranium	Facial cranium	Jaw areas	
219	Cranium	Facial cranium	Dental areas	
21a	Cranium	Facial cranium	Ramus area	
21b	Cranium	Facial cranium	Molar upper and lower jaw	
21c	Cranium	Facial cranium	Molar upper jaw	
21d	Cranium	Facial cranium	Third molar upper jaw	
21e	Cranium	Facial cranium	Molar lower jaw	
21g	Cranium	Facial cranium	Premolar upper and lower jaw	
21h	Cranium	Facial cranium	Premolar upper jaw	
21i	Cranium	Facial cranium	Premolar lower jaw	
21k	Cranium	Facial cranium	Canine upper jaw	
21l	Cranium	Facial cranium	Canine lower jaw	
21n	Cranium	Facial cranium	Incisor upper jaw	
21o	Cranium	Facial cranium	Incisor lower jaw	
Biology				
4a1	Gastrointestinal system	Salivary glands	Parotid gland	
4a3	Gastrointestinal system	Salivary glands	Mandibular gland	
c00	Dental system	Not further specified		
c10	Dental system	Dentulous system	Not further specified	
c20	Dental system	Edentulous system	Not further specified	
c30	Dental system	Implant system	Not further specified	

The Image Retrieval in Medical Applications coding scheme can be obtained from http://irma-project.org

Table 2 Image repository used in this study

		Total number of images								
No.	*IRMA category code*	*Absolute*	*Relative*	*1-1*	*1-2*	*1-3*	*1-4*	*2-1*	*2-2*	*Total number of individual frames*
1	111d-4c0-219-c10	238	11.90	238	0	0	0	0	0	238
2	111d-4c0-218-c10	188	9.40	188	0	0	0	0	0	188
3	1115-220-210-c10	84	4.20	84	0	0	0	0	0	84
4	111d-4c2-21a-c10	68	3.40	2	66	0	0	0	0	134
5	111d-4c0-219-c30	61	3.05	61	0	0	0	0	0	61
6	111d-4c1-21a-c10	54	2.70	3	51	0	0	0	0	105
7	1112-12g-214-c20	47	2.35	10	18	18	1	0	0	104
8	1115-220-200-c10	38	1.90	38	0	0	0	0	0	38
9	1112-12h-214-c20	38	1.90	9	19	10	0	0	0	77
10	1119-4c0-21n-c10	38	1.90	38	0	0	0	0	0	38
11	1115-120-210-c10	35	1.75	35	0	0	0	0	0	35
12	1119-4c2-21n-c10	35	1.75	35	0	0	0	0	0	35
13	111d-4c1-21l-c30	34	1.70	1	8	0	0	15	10	87
14	111b-312-215-c10	32	1.60	32	0	0	0	0	0	32
15	111d-4c2-21l-c30	32	1.60	2	6	0	0	13	11	84
16	1119-4c2-21l-c10	31	1.55	31	0	0	0	0	0	31
17	1119-4c1-21h-c10	30	1.50	30	0	0	0	0	0	30
18	1119-4c1-21e-c10	27	1.35	27	0	0	0	0	0	27
19	1119-4c1-21n-c10	27	1.35	27	0	0	0	0	0	27
20	1112-12g-215-c20	26	1.30	5	5	16	0	0	0	63
21	1119-4c1-21l-c10	26	1.30	26	0	0	0	0	0	26
22	1119-4c0-21o-c10	26	1.30	26	0	0	0	0	0	26
23	111d-4c1-215-c10	25	1.25	7	18	0	0	0	0	43
24	1119-4c2-21e-c10	25	1.25	25	0	0	0	0	0	25
25	1119-4c2-21k-c10	25	1.25	25	0	0	0	0	0	25
26	111b-4c2-21n-c10	25	1.25	25	0	0	0	0	0	25
27	1119-4c2-21h-c10	24	1.20	24	0	0	0	0	0	24
28	1119-4c1-21k-c10	24	1.20	24	0	0	0	0	0	24
29	111b-311-215-c10	23	1.15	23	0	0	0	0	0	23
30	1119-4c2-21i-c10	23	1.15	23	0	0	0	0	0	23
31	111d-4c2-210-c10	21	1.05	21	0	0	0	0	0	21
32	1112-12h-215-c20	21	1.05	6	3	11	1	0	0	49
33	111d-120-210-c10	20	1.00	20	0	0	0	0	0	20
34	111d-4c1-210-c10	20	1.00	20	0	0	0	0	0	20
35	1115-120-200-c10	19	0.95	19	0	0	0	0	0	19
36	111d-220-210-c10	19	0.95	19	0	0	0	0	0	19
37	1111-220-210-4a3	17	0.85	17	0	0	0	0	0	17
38	111d-4c1-214-c10	17	0.85	1	16	0	0	0	0	33
39	111d-12g-214-c30	17	0.85	0	17	0	0	0	0	34
40	111b-310-215-c10	17	0.85	17	0	0	0	0	0	17
41	1111-120-217-c10	17	0.85	17	0	0	0	0	0	17
42	111d-4c2-21i-c30	17	0.85	1	1	0	0	9	6	45
43	1111-210-210-4a1	16	0.80	16	0	0	0	0	0	16
44	1111-220-210-4a1	16	0.80	16	0	0	0	0	0	16
45	111d-4c1-21d-c10	16	0.80	1	12	0	0	0	3	37
46	111d-4c0-21o-c10	16	0.80	1	14	0	0	1	0	31
47	111d-4c2-215-c10	15	0.75	3	12	0	0	0	0	27
48	111a-4c2-21g-c10	15	0.75	15	0	0	0	0	0	15
49	1111-210-210-4a3	14	0.70	14	0	0	0	0	0	14
50	111d-220-210-c20	14	0.70	14	0	0	0	0	0	14
51	111a-4c1-21g-c10	14	0.70	14	0	0	0	0	0	14
52	1111-12g-210-4a1	13	0.65	13	0	0	0	0	0	13
53	111d-12h-214-c30	13	0.65	0	13	0	0	0	0	26
54	111a-4c2-21b-c10	13	0.65	13	0	0	0	0	0	13
55	111d-4c2-21d-c10	13	0.65	0	9	0	0	0	4	34
56	111d-4c2-21k-c30	13	0.65	3	7	0	0	1	2	27
57	111d-4c2-21l-c10	13	0.65	2	7	0	0	0	4	32
58	1111-210-216-c00	12	0.60	12	0	0	0	0	0	12
59	1111-220-216-c00	12	0.60	12	0	0	0	0	0	12
60	111d-4c0-219-c20	12	0.60	12	0	0	0	0	0	12
61	111b-4c0-21n-c10	12	0.60	12	0	0	0	0	0	12
62	111b-4c1-21n-c10	12	0.60	12	0	0	0	0	0	12
63	1111-320-200-c10	11	0.55	11	0	0	0	0	0	11
64	111d-4c2-214-c10	11	0.55	2	9	0	0	0	0	20
65	111a-4c1-21b-c10	11	0.55	11	0	0	0	0	0	11

(*continued on next page*)

Table 2 (*continued*)

		Total number of images								
No.	*IRMA category code*	*Absolute*	*Relative*	*1-1*	*1-2*	*1-3*	*1-4*	*2-1*	*2-2*	*Total number of individual frames*
66	1119-4c2-21c-c10	11	0.55	11	0	0	0	0	0	11
67	111d-4c1-21i-c30	11	0.55	1	1	0	0	7	2	25
68	111d-4c0-218-c30	10	0.50	10	0	0	0	0	0	10
69	111d-4c2-21h-c10	10	0.50	2	8	0	0	0	0	18
70	111d-4c1-21l-c10	10	0.50	1	6	0	0	0	3	25
71	1119-4c1-21i-c10	10	0.50	10	0	0	0	0	0	10
Sum		2000	100.00%	1526	326	55	2	46	45	2623

IRMA, Image Retrieval in Medical Applications

In order to provide sufficient training data, only categories with ten or more images were further evaluated. From the 2355 radiographs, 2052 images remained forming 71 classes. From each of the 2 most prominent classes, 26 images were randomly excluded such that the remaining subset held 2000 images. It turned out that from those, 474 were composed of more than one image field (Table 2). In particular, 326 images were composed of a row with 2 image fields (1-2), 55 images formed a row with 3 fields (1-3) and 2 images existed where 4 frames are placed within a row (1-4). Furthermore, 46 images were composed of a single row with 2 individual frames (2-1), and 45 images showed 4 individual radiographs placed in 2 rows of 2 columns (2-2).

In case the images were cut according to the field pattern and the original image was replaced by the respective image fields, the total number of references was 2623 (Table 2). However, 13 image fields which did not show a radiographic image were detected automatically by a simple analysis of the variance of grayscales and withdrawn from further investigation (see, for instance, Class 7 in Figure 2).

Disregarding the dental system, 65 classes remained. In other words, those classes were merged where the IRMA code TTTT-DDD-AAA-BBB only differed in the last two digits of the biosystem, and the first digit denotes the dental system, *i.e.* TTTT-DDD-AAA-c**. These are the dentulous, the edentulous, and the implant systems (Table 1). For example in Table 2, Class 1, Class 5, and Class 60 with IRMA code 111d-4c0-219-c10, 111d-4c0-219-c30, and 111d-4c0-219-c20, respectively, formed a new class 111d-4c0-219-c** with 310 images.

Table 2 summarizes the data finally used in this study. The most frequent images were panoramic radiographs of the dental regions with TTTT-DDD-AAA-BBB code (111d-4c0-219-c10) determining (X-ray imaging, plain radiography, digital, narrow beam radiography—other orientation, perpendicular to the dental arch—cranium, facial cranium, dental areas—dental system, implant system). According to the IRMA code, a zero states "not further specified" (Table 1). The last row with IRMA code 1119-4c1-21i-c10 indicates a right adjoining intraoral periapical radiograph of the mandibular premolar region. Figure 2 shows an example of an image taken arbitrarily from each of the classes. An image with multiple fields is shown in Classes 7, 39, 53 and 55. Class 7 also exemplifies the rare situation of not all panels of the multifield image being filled with a radiographic image.

According to the CBA paradigm, all dental radiographs were represented by a global set of numerical features. A combination of IDM, CCF and TTM was used,[11] where each classifier results in a distance $d(r,q)$ between the query and reference feature vector q and r, respectively. Let c denote a class and $R = \{r_i\}$, $R = \bigcup_{c=1}^{C} R_c$ the set of according reference vectors r. A parallel combination of distances yields

$$d_c(q,r) = \sum_{i=1}^{N} \lambda_i \cdot d_i'(q,r) \qquad (1)$$

where

$$d'(q,r) = \frac{d(q,r)}{\sum_{n=1}^{|R|} d(q,r_n)}$$

denotes the normalized distance, and $\lambda_i \in [0,1]$, $\sum_{i=1}^{N} \lambda_i = 1$ the weights each classifier contributes to the final result. Since the TTM represents each image by 384 numerical features, the radiographs are finally represented by 1408 or 640 feature values, when IDM and CCF are based on downsized images of 32×32 or 16×16 pixels, respectively.

Leaving-one-out experiments were performed in order to determine the rate of correct classification considering the best match, as well as the presence of the correct class within the five and ten best matching responses. More precisely, the following experiments were computed:

(A) The 2000 previously unseen dental radiographs were automatically annotated based on the combined classifier optimized on non-dental radiographs.[17]
(B) In another experiment, the weights were optimized to minimize the error rate on dental radiographs. Forced by a small number of images but a large number of classes, the 2000 reference images were used for both the tuning of the classifier and the final leaving-one-out evaluation.
(C) Using the setting of Experiment B, the classifier was applied to the six classes problem of automatically determining the number of image fields. According to the classifier's decision, all image fields are used to determine an average distance to the $2610 - x$ remaining references, where x denotes the respective number of individual fields. Based on this extended data, Experiments A and B were repeated.

Figure 2 Example images. The category numbers refer to the first column in Table 2

(D) Experiments A, B and C were performed on the remaining 65 classes disregarding the dental system, *i.e.* dentulous, edentulous and implant systems.
(E) Experiment C was performed on a set of 67 classes, which resulted from merging the dentulous and implant systems but maintaining the edentulous system in individual classes.

Results

Table 3 summarizes all experiments. Using the classifier where features and distances were optimized based on non-dental radiographs (Experiment A), the absolute error rate was 25.15%, which yields 9.05% and 4.05% if the correct class is selected among the five and ten best matches, respectively.

Table 3 Results

	Data set		*Weights*				*Error rate (%)*		
Experiment no.	*Images*	*Classes*	λ_{IDM}	λ_{CCF}	λ_{TTM}	*Number of features*	*Best match*	*Within five*	*Within ten*
A	2000	71	0.42	0.18	0.40	1408	**25.15**	**9.05**	**4.05**
						640	25.85	9.90	5.85
B			0.00	0.60	0.40	1408	**23.20**	**7.95**	**4.40**
						640	24.15	8.50	4.50
C	2610	71	0.42	0.18	0.40	1408	26.45	9.45	4.60
						640	27.85	10.70	6.65
			0.00	0.60	0.40	1408	**23.05**	**7.00**	**4.20**
						640	23.25	7.95	4.05
D	2000	65	0.42	0.18	0.40	1408	21.70	7.85	3.45
						640	23.00	8.75	5.20
			0.00	0.60	0.40	1408	**20.35**	**6.60**	**3.35**
						640	21.20	6.85	3.40
	2610	65	0.42	0.18	0.40	1408	22.90	8.25	4.05
						640	24.95	9.55	6.05
			0.00	0.60	0.40	1408	**20.05**	**5.65**	**3.25**
						640	20.35	6.55	3.35
E	2610	67	0.00	0.60	0.40	1408	**20.55**	**5.75**	**3.25**
						640	20.95	6.60	3.40
Non-dental	10000	57	0.42	0.18	0.40	1408	**12.60**	**5.60**	**3.60**
						640	14.30	5.80	4.10
	11000	117	0.42	0.18	0.40	1408	**21.50**	**10.00**	**7.30**

Error rates that are referred to from the body text are typeset in bold face

Using an optimized classifier based on the dental data (Experiment B), the relevant numbers were 23.20%, 7.95% and 4.40%, respectively. Reducing the length of the feature vector to less than a half resulted in an average increase of the error rate of one up to two percentage points.

Improvement was obtained using the automatic field pattern detection (Experiment C). The corresponding confusion matrix is shown in Table 4. Only six false positive and four false negative cuts were made. Thus, the error rate of field pattern detection was as low as 0.5%. The corresponding error rate yielded 23.05%, 7.00% and 4.20%, respectively.

Disregarding the dental system (Experiment D), the number of classes was reduced slightly from 71 to 65 (−8.5%). However, the error rate for the optimized classifier significantly decreased to 20.05% (−13.0%), 5.65% (−19.3%) and 3.25% (−22.6%), respectively.

This effect is maintained for the merge of dentulous and implant systems (Experiment E), which resulted in 67 classes (−5.6%) and 20.55% (−10.8%), 5.75% (−17.9%) and 3.35% (−20.2%) for the best match and within the five and ten best matches, respectively.

Considering the correct response within the ten best matches over all experiments, the lowest error rate of 3.25% and 3.35% was obtained for the optimized classifier based on the automatic field detection with 1408 and 640 feature values, respectively.

Discussion

The shift from mainly text-based data management to an image content-based processing is depicted as one of seven important developments for future medical information systems[18] and in the field of imaging informatics.[19] More precisely, CBIR has the potential to be an important factor in radiology.[20] Accordingly, automated image capturing, integration and analysis are needed for dental informatics.[21] With respect to computer-based oral health records, interinstitutional data collections will be established in the near future and used for evidence-based medicine.[22] However, CBA or CBIR techniques must be established in order to handle large repositories of medical image data. In particular for adaptive processing of such data repositories, automated categorization regarding the imaging modality and direction, the anatomic region, as well as the imaged biosystem is required on a much deeper level than provided within the DICOM header.[10,14,15]

Table 4 Confusion matrix of automatic field pattern detection

	Detected image fields						
True image fields	*1-1*	*1-2*	*1-3*	*1-4*	*2-1*	*2-2*	*Sum*
1-1	1520	6					1526
1-2	1	325					326
1-3			55				55
1-4			2				2
2-1					46		46
2-2	1					44	45

So far, CBA has been applied only in the field of non-dental diagnostic radiology. In a recent competition[6] where 10 000 non-dental radiographs of 57 classes were analysed, error rates in automated annotation of 12.6%, 5.6% and 3.6% were obtained to the correct class being the first, within the first five, or within the first ten best matches, respectively (Table 3). It is obvious that these figures are improved if the number of references is increased or the number of classes is decreased. Hence, increasing the number of classes yields 21.5%, 10.0% and 7.3%, respectively (Table 3). Since the data set used in this study contains only 2000 radiographs, it is not surprising that the error rates for the best match are also above 20% regardless of the type of classifier optimization, the number of features (1408 *vs* 640), or the number of classes (71 *vs* 65 or 67). However, if the error rate within the ten best matches is analysed, dental radiographs can be annotated even better than the non-dental (3.25% for 67/2610 *vs* 3.60% for 57/10 000).

Experiments D and E emphasise the difficulties of distinguishing dentulous and implant dental systems. While the relative decrease in classes is only 8.5% and 5.6%, the error rates decrease by 13.0% and 10.8%, which equals a factor of 1.5 and 1.9, respectively. These figures support our finding that dentulous and implant systems certainly overlap in terms of global texture features.

In conclusion, digital imaging has become the standard in dental radiology and comprehensive archives are being compiled. Automatic content analysis is required for efficient access to and sophisticated processing of the digital image data. The advantages of rapid access to specified types of image data in education, research and diagnostics are obvious. Global texture measures are capable of reflecting the image content. The correctness of automatic classification of dental image repositories is similar to non-dental. The quality of classification depends on the number of references used for training. Therefore, classification improves if composed sets of images (*e.g.* tomographic slices from premolar lower jaw) are decomposed into individual panels before the texture features are extracted, because this extends the *de facto* number of reference images. However, the disproportionate reduction of error rates observed in Experiments D and E result rather from particular problems of class similarity than from the decreased number of classes. Nonetheless, such problems can be solved by increasing the number of references. Using CBA access to dental image archives will certainly assist dental radiologists in finding appropriate diagnostic terms for the radiograph currently being read.

Acknowledgments
This work has been supported in parts by the Deutsche Forschungsgemeinschaft DFG, grant Le 1108/4.

References

1. Smeulders AWM, Worring M, Santini S, Gupta A, Jain R. Content-based image retrieval at the end of the early years. *IEEE Trans Pattern Anal Mach Intell* 2000; **22:** 1349–1380.
2. Tagare HD, Jaffe CC, Duncan J. Medical image databases—a content-based retrieval approach. *J Am Med Inform Assoc* 1997; **3:** 184–198.
3. Tang LHY, Hanka R, Ip HHS. A review of intelligent content-based indexing and browsing of medical images. *Health Inform J* 1999; **5:** 40–49.
4. Müller H, Michoux N, Bandon D, Geissbuhler A. A review of content-based image retrieval systems in medical applications—clinical benefits and future directions. *Int J Med Inform* 2004; **73:** 1–23.
5. Niblack W, Barber R, Equitz W, Flickner M, Glasman E, Petkovic D, et al. The QBIC project—querying images by content using color, texture, and shape. *Proc SPIE* 1993; **1908:** 173–187.
6. Clough P, Müller H, Deselaers T, Grubinger M, Lehmann TM, Jensen J, et al. The CLEF 2005 cross language image retrieval track. *Lect Notes Comput Sci* 2006; **4022:** 535–558.
7. Haralick RM, Shanmugam K, Dinstein I. Textural features for image classification. *IEEE Trans Syst Man Cybern* 1973; **3:** 610–621.
8. Tamura H, Mori S, Yamawaki T. Textural features corresponding to visual perception. *IEEE Trans Syst Man Cybern* 1978; **8:** 460–472.
9. Keysers D, Dahmen J, Ney H, Wein BB, Lehmann TM. A statistical framework for model-based image retrieval in medical applications. *J Electronic Imaging* 2003; **12:** 59–68.
10. Lehmann TM, Güld MO, Thies C, Fischer B, Spitzer K, Keysers D, et al. Content-based image retrieval in medical applications. *Methods Inf Med* 2004; **43:** 354–361.
11. Lehmann TM, Güld MO, Deselaers T, Keysers D, Schubert H, Spitzer K, et al. Automatic categorization of medical images for content-based retrieval and data mining. *Comput Med Imaging Graph* 2005; **29:** 143–155.
12. Deselaers T, Müller H, Clough P, Ney H, Lehmann TM. The CLEF 2005 automatic medical image annotation task. *Int J Comp Vis* 2006 online first, DOI: 10.1007/s11263-006-0007-y.
13. Lehmann TM, Bredno J. Strategies to configure image analysis algorithms for clinical usage. *J Am Med Inform Assoc* 2005; **12:** 497–504.
14. Güld MO, Kohnen M, Keysers D, Schubert H, Wein BB, Bredno J, et al. Quality of DICOM header information for image categorization. *Proc SPIE* 2002; **4685:** 280–287.
15. Traina JC, Traina AJM, Araujo MRB, Bueno JM, Chino FJT, Razente H, et al. Using an image-extended relational database to support content-based image retrieval in a PACS. *Comput Methods Programs Biomed* 2005; **80:** 71–83.
16. Lehmann TM, Schubert H, Keysers D, Kohnen M, Wein BB. The IRMA code for unique classification of medical images. *Proc SPIE* 2003; **5033:** 109–117.
17. Güld MO, Thies C, Fischer B, Lehmann TM. Content-based retrieval of medical images by combining global features. *Lect Notes Comput Sci* 2006; **4022:** 702–711.
18. Haux R. Health information systems—past, present, future. *Int J Med Inform* 2006; **75:** 268–281.
19. Sinha U, Bui A, Taira R, Dionisio J, Morioka C, Johnson D, et al. A review of medical imaging informatics. *Ann NY Acad Sci* 2002; **980:** 168–197.
20. Müller H, Rosset A, Garcia A, Vallee JP, Geissbuhler A. Benefits of content-based visual data access in radiology. *Radiographics* 2005; **25:** 849–858.
21. Sittig DF, Kirshner M, Maupome G. Grand challenges in dental informatics. *Adv Dent Res* 2003; **17:** 16–19.
22. Eisner J. The future of dental informatics. *Eur J Dent Educ* 1999; **3:** 61–69.